JOURNAL OF OPTOELECTRONICS AND ADVANCED MATERIALS Vol. 12, No. 2, February 2010, p. 177 - 183

β - $FeSi_2$ and Schottky barrier at Fe/Si interface

CHHAGAN LAL, RENU DHUNNA, R. S. DHAKA[a], S. R. BARMAN[a], I. P. JAIN[*]
Centre for Non-Conventional Energy Resources, University of Rajasthan, Jaipur, India
[a]*UGC-DAE-CSR, Khandwa Road, Indore, 452001, India*

Metal / semiconductor interface investigations have been of enormous research interest because of technological application in microelectronics. In the present work Fe films deposited on Si(111) substrate were studied as a function of annealing temperatures for the formation of silicide phases. Grazing incidence x-ray diffraction (GIXRD) results show a stable disilicides β-$FeSi_2$ formation at the interface at 600^0 C. The coercivity, determined by Magneto Optical Kerr Effect (MOKE) technique shows a hysteresis curves for as-deposited and annealed samples which varies from 14.914 Oe to 31.016Oe. The coercivity of β-$FeSi_2$ is higher than of pristine sample which is due to the formation of nanocrystalline grains with increasing annealing temperatures. X-ray photoelectron spectroscopy study shows shifting of Fe2$P_{3/2}$ peak towards higher binding energy for annealed samples. The Schottky barrier height by the *I-V* measurement varies from 0.59eV to 0.49 eV.

(Received January 25, 2010; accepted February 18, 2010)

Keywords: X-ray photoelectron spectroscopy, Electrical transport measurements, Metal-semiconductor interfaces, Schottky barrier, Thermionic emission

1. Introduction

Interface studies in metal/semiconductor systems are important due to their potential technological application in microelectronics [1]. Fe/Si systems have been studied extensively as its applications in the development of magnetic silicon based heterostructures, because of its abnormal magnetic and transport behaviors. These thin films show antiferromagnetic coupling [2] similar to as observed in metal/metal thin films. Refractory metal/Si multilayer structures are of research interest for making electrical interconnects as well as in basic research [3].

The iron silicide phases at Fe/Si interfaces are formed by interdiffusion and intermixing at room temperature or by annealing of the samples at elevated temperatures [4,5]. The silicides can be classified, according to their formation kinetics from a metallic thin film and silicon substrate by conventional solid phase reaction. The most important type of kinetics is the diffusion-controlled reactions. All diffusion-controlled reactions have an initial stage under a certain thickness, where they exhibit reaction-controlled growth kinetic [6]. The next category of kinetics is the nucleation-controlled reactions, where nucleation is so difficult that it dominates the process of phase formation [7]. As reported in literature [8 – 12], following phases of the Fe-Si equilibrium phase diagram have been found in thin film reactions, mainly on Si(111) substrate:

a. Fe_3Si is the Fe – rich silicide with cubic structure.

b. Two types of iron monosilicide may appear in thin film form, the first phase is ε-FeSi with cubic structure and the second monosilicide phase is cesium-chloride type cubic FeSi. The iron disilicides, prepared in thin layers, might have three different crystal structures;

i. The high temperature, metastable, tetragonal α - $FeSi_2$ phase may be epitaxially stabilized in thin film form on Si substrates;

ii. The cubic γ – $FeSi_2$ phase is also a metastable structure and

iii. The β – $FeSi_2$ has orthorhombic structure.

The above mentioned phases, including metastable ones, may be epitaxially stabilized on the surface of Si(111) substrate. Dependence of solid – phase growth of β – $FeSi_2$ thin films on the crystal orientation of Si substrates has been investigated by using a – Fe/c-Si (100), (110) and (111) stacked structures [13]. XRD measurements suggested that the substrate orientation dependence of the formation rate of β – $FeSi_2$ follows as (100) > (111) > (110) and can be explained on the basis of the lattice mismatch between β – $FeSi_2$ and Si substrates.

The characteristics at the interface are dictated by interdiffusion thickness, uniformity of interdiffusion parallel to interface and the structural properties at the interface. Many previous structural studies are important for the information about the crystalline nature of Fe layer and amorphous Si spacer layer [2, 14]. The formation of iron silicide and its crystalline structure in spacer layer region is reported for the sputtered Fe/Si multilayer by Strijkers et al. [15] According to them Fe/Si and Si/Fe interfaces are not equivalent with respect to the formation of iron silicide. Fe/Si interface studied by depositing Fe on crystalline Si substrate [16 – 18] was found to be different from actual thin film structure. Depending on the Fe

thickness and on the annealing temperature, stable ε-FeSi, β – $FeSi_2$ and metastable disordered, c-FeSi phases were formed [19]. After annealing, metastable c-FeSi, stable ε – FeSi and at higher temperature stable β – $FeSi_2$ phases were formed. The valance band photoemission have been used to study the thin Fe films on Si (001) and compared with that of pure Si and the highest Fe film thickness. All these different spectra for all thickness show almost similar shape indicating the same origin i.e the Fe/Si interface [20].

Refractory silicides RSi_2 have high-temperature stability and high electrical conductance [21]. Low specific contact resistivities of 10^{-8} Ωcm^2 are essential to realize ULSI's, which have very small contact holes of the order of 0.1 mm in size [22]. The silicides–silicon interface is of paramount importance for basic purpose and future technological applications [23. 24]. Of particular interest are the initial stages of the interface development during metal deposition at room temperature because the interdiffusion induces the formation of various silicides compounds [25, 26] and thus influences the stability of such interfaces. From the available literature on silicon–iron–silicide system: the epitaxy of the semiconducting β - phase has been characterized as a three-domain growth of the orthorhombic b-phase lattice with β-$FeSi_2$(101); Si(111) or β-$FeSi_2$(110); Si(111) [27]. The larger density of structural defects for this interface (domains) could not provide applications of this system to the development of infrared detectors of all-silicon technologies. Evidence of a cubic silicides with a CsCl-type lattice and stoichiometries ranging from FeSi to $FeSi_2$ have also been obtained [28], which clearly shows the possibility of growing lattice matched metastable phases of iron silicides on the Si(111) surface.

In the present paper studies on iron thin films on Si substrate have been reported which has been fabricated using an electron beam evaporation method and annealed at different annealing temperatures for the formation of various phases at the interface and characterized by Grazing incidence x-ray diffraction (GIXRD) technique. The chemical composition and chemical shift have been studied using x-ray photoelectron spectroscopy (XPS). *I-V* curves are taken at different temperatures for the samples annealed at different temperatures. Schottky barrier height (SBH) and heat of formation have been investigated.

2. Experimental

The n-type Si(111) of area 1x1 cm^2 and of thickness 500 μm have been used as a substrates to grow the thin films. The substrates were initially chemically cleaned by a conventional procedure (TCE, acetone, methanol) and then dipped into a diluted HF (1:10) solution to remove impurities or any oxide layer present before loading into vacuum chamber. The time taken between the cleaning of substrate and loading into the vacuum chamber was kept less than 90 sec. Fe film of 80nm was deposited on Si(111) substrate using electron beam evaporation technique at room temperature and in a vacuum of $2x10^{-7}$ torr keeping a deposition rate of 32 Å/min. The samples were annealed at 500 and 600^0C temperatures for 1 hour in $3x10^{-5}$ torr vacuum for the formation of silicide phases.

3. Results and discussion

3.1 Structural study

As deposited and after annealing at different temperatures, the samples were studied by using GIXRD to confirm the presence of phase formation or crystal structure at the interface. GIXRD measurements by using CuKα (λ = 1.54 Å) radiations were recorded in the 2θ range of 20–80^0 to identify the phases. Fig. 1a shows the diffraction pattern of as-deposited bilayer system and gives separate crystalline peaks corresponding to Fe(110), Fe(200) and Si(111). It does not show the formation of any silicide which means that Fe film is chemically stable on Si under the above condition. After annealing at higher temperatures, this system shows crystalline peaks of Fe as well as Bragg peaks corresponding to different planes of FeSi and $FeSi_2$, due to the interfacial reaction occurring at 500 and 600^0C. Figure 1b shows the pattern of Fe/Si sample annealed at 500^0C. It shows formation of crystalline FeSi(210) and FeSi(222). GIXRD measurement on the same system after annealing at 600^0C, leads to the formation of β-$FeSi_2$(402) and β-$FeSi_2$(224) phases, as shown in Fig. 1c. The crystal structure of FeSi and $FeSi_2$ are cubic & orthorhombic respectively. The experimental peak positions are compared with the literature and corresponding Miller indices were indexed. All the measurements show that intensity of Fe(110) and Fe(200) decreases, with increase in annealing temperature resulting an interfacial reactions for the formation of silicides. The x-ray diffraction is sensitive to the crystallite size. From the well known Scherrer formula, the average crystallite size (D) is given [29] as

$$D = \left(\frac{0.9\lambda}{\beta(Cos\theta)} \right) \quad (1)$$

where λ is the x-ray wavelength, θ is the diffraction angle and β is the line width of the diffraction profile resulting from small crystallite size. Using above equation, the crystallite size of $FeSi_2$ phase was calculated and it was equal to 74.55 Å ± 0.02 Å.

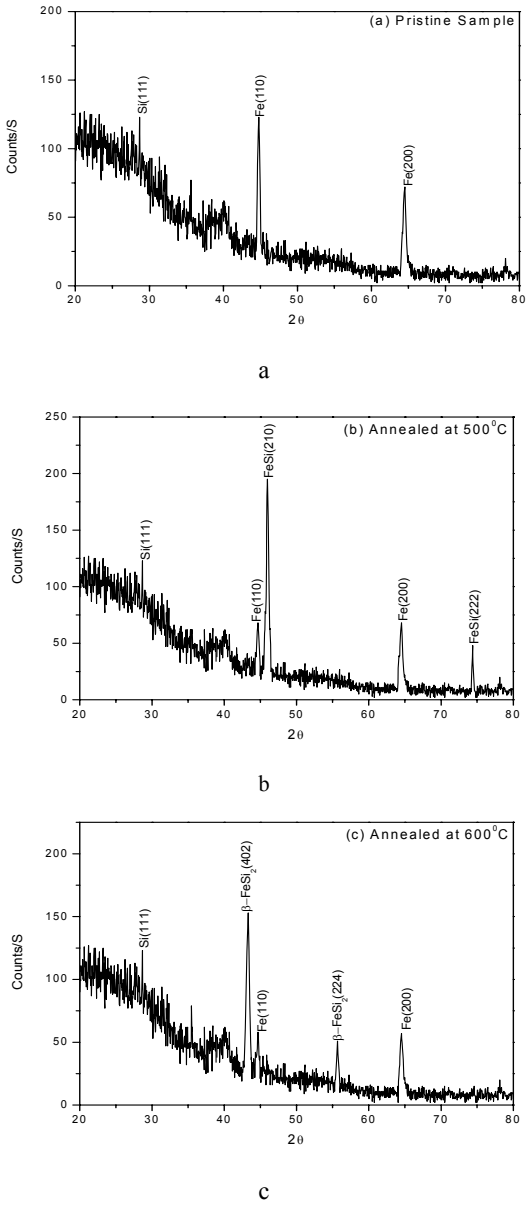

Fig 1. a. GIXRD pattern of Fe/Si as deposited sample, b. GIXRD pattern of Fe/Si annealed at 500 ^{0}C, c. GIXRD pattern of Fe/Si annealed at 600 ^{0}C.

3.2 Magnetic properties

The magnetic properties of the samples were characterized by ex-situ Magneto Optical Kerr Effect (MOKE) at room temperature. The MOKE system consists of a polarized He–Ne 10mW laser source operating at 623.8 nm, two polarizers, a photoelastic modulator and a photodiode detector. Measurements in the longitudinal geometry were performed with the magnetic field of 800 Oe applied in the plane of incidence (parallel magnetization). Figures 2a–c show the magnetization measurements carried out using the MOKE technique for as-deposited Fe/Si thin film and annealed samples at 500 and 600^{0}C. Hysteresis loop measurements have been characterized by the coercivity Hc, which can be defined as the displacement at the half-width of the loop. From recorded hysteresis loops, it has been observed clearly that all the samples show well-saturated magnetization with applied magnetic field. The coercivity value determined from the MOKE hysteresis curve for as-deposited sample has been found to be 14.914 Oe, and for other annealed samples at 500 and 600^{0}C it is 29.825 and 31.016 Oe, respectively.

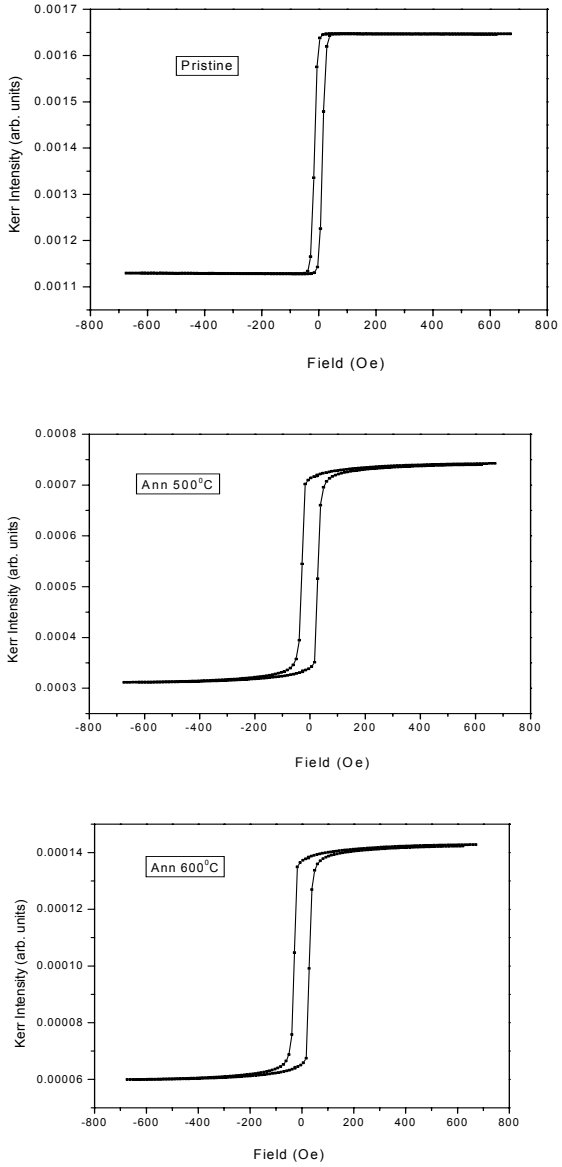

Fig. 2. a. Longitudinal Kerr signal versus Applied Magnetic field of Fe/Si pristine System. b. Longitudinal Kerr signal versus Applied Magnetic field of Fe/Si annealed sample at 500^{0}C. c. Longitudinal Kerr signal versus Applied Magnetic field of Fe/Si annealed sample at 600 ^{0}C.

The coercivity of β-$FeSi_2$ is higher than the coercivity of pristine sample, which is due to the formation of

nanocrystalline grains with increasing annealing temperatures [30]. It is evident from *I– V* characteristics because resistance of annealed samples abruptly decreases, i.e. the conductivity of annealed samples increases due to the formation of nanocrystalline grains. It is also observed from GIXRD results that the particle size is of nanometer range, indicating the formation of nanocrystalline grains.

3.3 Photoemission measurements:

The surface chemical composition and the binding energy shift have been studied by using X-ray photoelectron spectroscopy (XPS). XPS is an analytical technique depending upon the energies of photoelectrons emitted from the atoms when they are irradiated by X-ray photons. A commercial electron energy analyzer (Phoibos100 from Specs GmbH, Germany) and a non-monochromatic Mg Kα (hν = 1253.6 eV) line as the X-ray source were used under the condition of an ultra high vacuum (~ 1×10^{-10} torr). The chemical composition and core-levels of as-deposited Fe/Si and after annealing were studied. These samples of Fe/Si were cleaned by light sputtering in the XPS chamber to remove the contamination. Since this is very surface sensitive technique and the sensitivity is enhanced when the photoelectron signals are detected in the grazing emission geometry [31, 32]. The interfaces may be analyzed when the top layer was Si – or Fe – rich which is in agreement with Orlowski et al. [33]. According to them no clear differences were observed for different interfaces including that of Fe 2*P* spectra. A wide scan of XPS spectra from 0 to 1200 eV was taken and no unwanted feature has been observed. Fig. 3a shows Fe 2*P* core-level spectrum and the binding energy (BE) of the spin orbit split peaks are 705.98 eV ($2P_{3/2}$) and 719.43 eV ($2P_{1/2}$) showing metallic features with line shape and BE position corresponds to the pure iron Fe 2*P* peaks [34]. The Fe $2P_{3/2}$ and Fe $2P_{1/2}$ signals are strong, marked by 1 and 2 as shown in Fig. 3a. The amount of FeO_x species can be derived from the extra component observed in Fe 2*P* peak at about 711.57 eV BE (marked by 3; corresponding to FeO_x). In Fig. 3b the spectra of Fe 2*P* after annealing treatment at different temperatures are shown. Orlowski et al. [33] reported that the spectra of pure iron after annealing at 350^0C do not show significant changes to prove the formation of iron silicide. For the present case, after annealing at 500^0C the Fe $2P_{3/2}$ peak has been observed at about 707.5 eV which is shifted towards higher BE by about 1 eV as compared to as deposited sample. Further annealing shift the peak towards higher BE (BE=707.7 eV at 550^0C) and at 600^0C the BE is about 708.3 eV. Since the core-level positions depend on the chemical state of the atoms and the changes in local environment and potential of an atom cause shifts in the core-level binding energies. By the appearance of the plasmon loss peak in the Fe 2*P* spectra the silicide formation can be recognized. The plasmon losses appearing at higher BE (low kinetic energy) of Fe *LVV* Auger peak after annealing at 500^0C is used in literature [35] to identify the chemical composition of the silicide. Features of this peak like relative intensity and BE in comparison to the parent peak vary for different silicide phases. The obtained value of plasmon loss energy of about 21.5 eV is in agreement with the iron monosilicide. Silicide formation involves dynamical processes (e.g. atomic diffusion and chemical reaction). Due to the annealing effect, the time constants of these processes should play an important role in the type of phases grown. An exact definition of the annealing procedure is crucial for a reproducible determination of the regions of coverage and temperature which give rise to a particular phase.

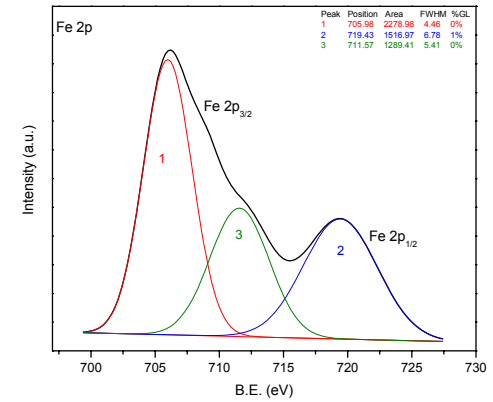

a

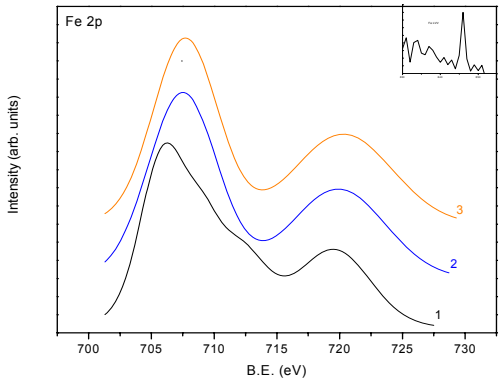

b

Fig. 3. a. Typical Fe $2P_{3/2}$ core-level spectrum at Fe/Si surface.b. Fe $2P_{3/2}$ core-level spectra at the Fe/Si surface for pristine and annealed at 500 and 600°C (marked by 1, 2, and 3 respectively).

3.4 Electrical measurements

The current across a metal-semiconductor junction is mainly due to majority carriers. For electrical measurements the silver paste is applied on the top and bottom to make contact on the sample. *I-V* characteristics have been measured for as-deposited and annealed samples using Keithely Electrometer - 6517A. Fig. 4a shows the typical *I-V* curve of Fe/Si system for as-

deposited and annealed samples at 500 & 600^{0}C. The requirement that the Fermi level matches up, results in potential barrier to transfer charges between metal and semiconductor and such a barrier is referred as Schottky barrier. Electrons overcome the potential barrier between the semiconductor and the metal through a quantum-mechanical process called thermionic emission. This process is activated by the thermal energy of the electrons. Although the potential barrier is clearly larger than kT/q at room temperature, so there exists a non-zero probability that some electrons gather enough energy to overcome the barrier. When a forward bias V_a is applied to the device, the potential barrier (the electrons have to overcome to transit from the semiconductor into the metal) is equal to ϕ_b '-V_a. The resulting thermionic emission current is given by

$$I_{m \to s} = A R^* T^2 \exp\left[-\frac{q\left(\Phi_b' - V_a\right)}{kT}\right] \qquad (2)$$

where R^* is called the Richardson constant which is equal to $4\Pi m_e q k^2/h^3$ and A is the Schottky diode area. Because of the dependence of the potential barrier height on the applied bias and generation/recombination in the depletion zone, the forward current takes the following form,

$$I = A R^* T^2 \exp\left[-\frac{q\Phi_b'}{kT}\right]\left[\exp\left(\frac{qV_a}{nkT}\right) - 1\right] \qquad (5)$$

or $$I = I_s\left[\exp\left(\frac{qV_a}{nkT}\right) - 1\right]$$

where $$I_s = AR^*T^2 \exp\left[-\frac{q\Phi_b'}{kT}\right]$$

The value of n such as $1 \le n \le 2$ is called the ideality factor of the diode which is larger than one when other carrier transport mechanisms, such as tunneling are involved [36]. Schottky diodes are capable of very fast switching because their operation is based on majority carriers unlike PN junction diodes where device operation is slowed down by storage and recombination of excess minority carriers. Majority carriers have a relaxation time on the order of tens of ten picoseconds, which allows for operation at frequencies up to tens of gigahertz.

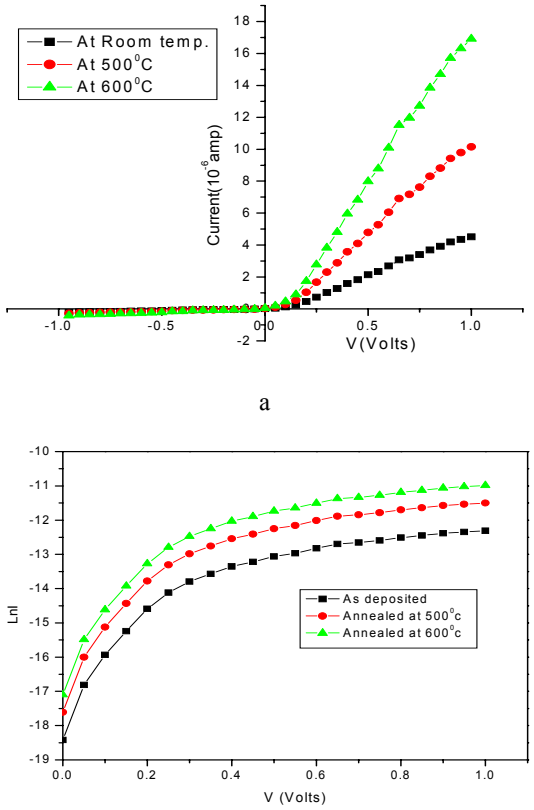

Fig. 4 a. Typically I-V curves for Fe/Si system at different annealing temperatures. b. Typically lnI vs V curves for Fe/Si system for as deposited and annealed samples at 500 and 600 ^{0}C.

In the present case it is assumed that current transport dominates the thermionic emission and barrier height is extracted by fitting a straight line in the linear portion of the semi logarithmic *I-V* curve having the effective mass of the electron in Si to be m*=0.26m$_0$. The value of I_s has been calculated from extrapolating the linear region of the *lnI* vs *V* as shown in Fig. 4b. Andrewe and Phillips [37] plotted the ϕ_b' values as a function of the heat of formation (ΔH) of the silicide. The result is defined by the following equation

$$\phi_b' = 0.83 + 0.18\ (\Delta H) \qquad (4)$$

The *lnI* vs *V* characteristics are linear at low forward bias voltages. The linearity of this curve is due to the effect of series resistance. The series resistance is significantly in downward curvature of forward bias *I-V* characteristics, but the two parameters are significant in both the linear and nonlinear regions of *I-V* characteristics. The calculated values of barrier heights are 0.59, 0.54 and 0.49 eV for as-deposited, annealing at 500 and 600^{0}C,

respectively. It is clear from the curves that the *SBH* decreases with increasing the annealing temperature. According to Fermi level pinning model of Bardeen [38], when the interface state density increases from Schottky limit to Bardeen limit, the *SBH* decreases. One thereby concludes that annealing causes an increase in interface state density leading to decrease in *SBH* with the formation of stable iron disilicide β-$FeSi_2$ and the *SBH* values as a function of heat of formation of silicides. The values of calculated heat of formation are -1.88, -1.55, -1.33 eV for as-deposited, annealed at 500 and 600^0C, respectively.

4. Conclusions

The photovoltaic application of orthorhombic $FeSi_2$ (β-$FeSi_2$) is one of its promising directions, as well as its application to optoelectronics devices because of its large optical absorption nature, a direct band-gap of ~ 0.87 eV smaller than indirect band-gap of 1.12 eV in Si, and furthermore, the non-toxicity of the compounds and low-cost resources of Si and Fe, etc. β -$FeSi_2$ is a new type of a semiconductor compatible with silicon technology and has drawn a considerable interest in recent years. In particular, the success in fabricating a light-emitting β –$FeSi_2$/Si diode operating at a wavelength of 1.5 μm renewed the interest in this material.

Structural, magnetic and electrical properties of silicide formation at Fe/Si interface due to annealing have been investigated by GIXRD, MOKE and *I-V* characteristics. GIXRD results revealed a stable disilicides β-$FeSi_2$ formation at the interface at annealing temperature of 600^0C. The coercivity of β-$FeSi_2$ is higher than the coercivity of as- deposited sample which is due to the formation of nanocrystalline grains with increasing annealing temperatures. The surface chemical composition and the binding energy shift have been observed by photoemission measurements. Typical Fe 2*P* core level spectrum at Fe/Si shows the metallic features: the shape of the peak Fe $2P_{3/2}$ and its binding energy is 705.98 eV, which corresponds to the pure iron Fe $2P_{3/2}$ has been analyzed peak. After annealing, the Fe$2P_{3/2}$ peak found to be shifted towards the higher binding energy. A significant increase in current has been observed after annealing. The Schottky barrier height is estimated by the current-voltage measurements and found to vary from 0.59 to 0.49 eV. It has also been observed that all the annealed samples have less Schottky barrier height than as-deposited. The Schottky barrier height decreases with decrease in the heat of formation of the silicides. Such types of studies are important for understanding the structural and magnetic properties of Fe/Si interface.

Acknowledgement

One of the authors is grateful to BRNS (DAE) Mumbai for financial support for this work. Authors are grateful for the financial support in the form of a project by BRNS (DAE). We are thankful to UGC-DAE-CSR for providing XPS and MOKE facilities for this work.

References

[1] W. C. Chen, C. H. Lai, S. F. Lee, Y. T. Cheng, Y. D. Yao, J. Magn. Magn. Mater. **239,** 319 (2002).
[2] A. Chaiken, R. P. Michel and M.A. Wall, Phys. Rev. **B53**, 5518 (1996).
[3] A. Chaiken, R.P. Michel and C.T. Wang, J. Appl. Phys. **79**, 4772 (1996).
[4] N. D. Telling, C. A. Faunce, M. J. Bonder, P. J. Grundy, D. G. Lord, S. Langridge, J. Appl. Phys. **89**, 7074 (2001).
[5] M. De Crescenzi et al, Phys. Rev. **B42**, 5871 (1990).
[6] U. Gosele, K. N. Tu, J. Appl. Phys. **53**, 3252 (1982).
[7] F. M. d' Heurla, J. Mater. Res. **3**, 167 (1988).
[8] H. Von Kanel, K. A. Mader, F. Muller, N. Onda, H. Sirringhans, Phys. Rev. **B45**, 13807 (1992).
[9] C. Lal, R. Dhunna, I.P. Jain, Vacuum **83**, 931 (2009).
[10] C. Lal, R. Dhunna, I.P. Jain, Materials Science in Semiconductor Processing **11**, 1 (2008).
[11] K. A. Mader, H Von Kanel, A. Baldereschi, Phys. Rev. **B48**, 4364 (1993).
[12] N. Jedrecy, A. Waldhaner, M. Sauvage – Simkin, R. Pinchaux, Y. Zheng, Phys. Rev. **B49**, 4725 (1994).
[13] Y. Murakami, A. Kenjo, T. Sadoh, T. Yoshitake, M. Miyao, Thin Solid Films **461**(1), 68 (2004).
[14] E. E. Fullerton, J. E. Mattson, S. R. Lee, C. H. Sowers, Y. Y. Huang, G. Felcher, S. D. Bader, J. Magn. Magn. Mater. **117**, L301 (1992).
[15] G. J. Strijkers, J. T. Kohlhepp, J. J. M. Swagten, W. J. M. Jonge, Phys. Rev. **B60**, 9583 (1999).
[16] R. Klasges, C. Carbone and W. Eberhardt, Phys. Rev. **B56**, 10801 (1997).
[17] K. Ruhrnschopf, D. Borgmann, G. Wedler, Thin Solid Films **280**, 171 (1996).
[18] B. Li, M. Ji, J. Wu, J. Appl. Phys. **68**, 1099 (1990).
[19] X. Gao, D. Qi, S.C. Tan, A.T.S. Wee, X. Yu, O. Moser Herbert, J. Ele. Spect. & Relt. Pheno. **151**(3), 199 (2006).
[20] L. Dezsi, Cs Fetzer, L. Szucs, J. Dekoster, A. Vantomme, M. Caymax, J. Surf. Sci. **599**(1-3), 122 (2005).
[21] M. Ekman, V. Ozolins, Phys Rev **B57**, 4419 (1998).
[22] T. Yamauchi, S. Zaima, K. Mizuno, H. Kitamura, Y. Koide, Y. Yasuda, J Appl Phys **69**, 7050 (1991).
[23] L. Brillson, Surf Sci **168**, 171 (1986).
[24] C. Calandra, O. Bisi, G. Ottaviani, Surf Sci Rep **4**, 271 (1985).
[25] J. Derrien, Surf Sci **168**, 171 (1986).
[26] J. Derrien, F. Arnaud d'Avitaya, J Vac Sci Technol **A5**, 2111 (1987).
[27] N. Jedrecy, Y. Zheng, A. Waldhauer, M. Sauvage-Simkin, R. Pinchaux, Phys Rev **B48**, 8801 (1992).
[28] Von Kanel H, K.A. Mader, E. Muller, N. Onda, H. Sirringhaus, Phys Rev B **45**, 13807 (1992).
[29] S. N. Danilchenko, O. G. Kukharenko, C. Moseke, I. Yu. Protsenko, L.F. Sukhodub and B. Sulkio-Cleff, Cryst. Res. Technol. **37**(11) 1234 (2002) .

[30] B. Majumdar, D. Akhtar, Bull Mater Sci **28**(5), 395 (2005).
[31] C. Biswas, A. K. Shukla, S. Banik, V. K. Ahire, S. R. Barman, PRB, **67**, 165416 (2003).
[32] R. S. Dhaka, S. W. D'Souza, M. Maniraj, Aparna Chakrabarti, D. L. Schlagel, T. A. Lograsso, S. R. Barman, Surface Science, **603**, 1999 (2009).
[33] B. A. Orlowski, B. J. Kowalski, K. Fronc, R. Zuberek, S. Mickevicius, F. Mirabella, J. Ghijsen, J. Alloys and Compounds **362**, 202 (2004).
[34] J. F. Moulder, W. F. Sticle, P. E. Sobol, K. D. Bomben, Physical Electronic Inc. Eden Prairie, Minnesota, USA, 1995.
[35] B. Egert, G. Panzer, Phys. Rev. B **29,** 2091 (1984).
[36] L. S. Yu, Q.Z. Liu, D. J. Qiao, S. S. Lau, J. M. Redwing, J. Appl. Phys. **84,** 2099 (1998).
[37] J. M. Andrewe, J.C. Phillips, Phys. Rev. Lett. **35**, 56 (1975).
[38] J. Bardeen, Phys. Rev. **71**, 717 (1947).

*Corresponding author: clsaini52@hotmail.com